On the development of a sliding mode observer-based fault diagnosis scheme for a wind turbine benchmark model

Authors

Mostafa Rahnavard [a]
Mohammad Reza Hairi Yazdi [a]
Moosa Ayati [a*]

[a] School of Mechanical Engineering, University of Tehran, Tehran, Iran

ABSTRACT

This paper addresses the design of an observer-based fault diagnosis scheme, which is applied to some of the sensors and actuators of a wind turbine benchmark model. The methodology is based on a modified sliding mode observer (SMO) that allows accurate reconstruction of multiple sensor or actuator faults occurring simultaneously. The faults are reconstructed using the equivalent output error injection signal. A well-known validated wind turbine benchmark model, developed by Aalborg University and KK-electronic a/c, is utilized to evaluate the FDD scheme. Different sensors and actuator fault scenarios are simulated in the drive train, generator, and pitch & blade subsystems of the benchmark model, and attempts have been made to estimate these faults via the proposed modified SMO. The simulation results confirm the effectiveness of the proposed diagnosis scheme, and the faults are well detected, isolated, and reconstructed in the presence of the measurement noise.

1. Introduction

Wind turbines are the most growing renewable energy systems excited by a completely random wind profile. Nonlinear dynamics, operation in uncertain environments, and experiencing large disturbances are the highlighted characteristics of these systems [1]. Despite applying advanced technology in the design and manufacturing of the wind turbine, the maintenance of today's wind turbines is still time-consuming and expensive [2]. Advanced fault diagnosis and fault-tolerant schemes implemented in the modern wind turbine can result in high reliability and efficient operation, and, accordingly, produce economically justifiable electrical energy [3-4].

*Corresponding author: Moosa Ayati
Address: School of Mechanical Engineering, University of Tehran, Tehran, Iran
E-mail address: m.ayati@ut.ac.ir

Hardware sensor-based and model-based methods are the most common fault diagnosis schemes implemented in the wind turbine [5]. In the sensor-based method, some system characteristics, such as temperature, vibration, and acoustic emission, among others, are monitored and analysed with the use of some expensive sensors [6-7].

In the analytical model-based method, a mathematical model by the help of sensor's measurements is used to continuously monitor wind turbines. Hence, many works have been performed on model-based fault diagnosis of wind turbines in recent years, following the presentation of the wind turbine benchmark model developed by Odgaard et al. [3], [8]. Some of these papers are reviewed in the following.

In [9] and [10], Kalman filter (KF)-based approaches for fault detection and isolation

14

(FDI) are presented. These approaches use the KF and generalized likelihood ratio test for residual generation and evaluation. Laouti et al. proposed an FDI scheme based on a combination of Kalman-like observer and support vector machines [11]. The FDI scheme was evaluated using a wind turbine benchmark with a real wind sequence. Robust residual filtering and parity equations were combined to propose an FDI scheme in [12].

Estimation of the effective wind speed is highly important as the wind speed sensors provide quite noisy measurements [5]. A wind speed estimator has been proposed in [13] to provide an effective wind speed. The FDI scheme utilizes a set-membership method to detect and isolate some faults in a wind turbine model. Estimation of the effective wind speed is also found in [13-14].

In [15-16], the unknown input observer is proposed for the detection of sensor faults in the drive train and converter subsystems of the benchmark model. An adaptive actuator fault estimation scheme is proposed by Simani et al., which is designed via the nonlinear geometric approach. Reconstruction of the actuator faults provided by adaptive filters is exploited to generate the residuals [18], [19].

Sliding mode observers (SMOs) benefit from the robustness to disturbances and modelling uncertainties. For this reason, the FDD schemes using SMO have recently been investigated thoroughly [20]-[24].

In [25], an SMO for the FDI of sensor faults in a wind turbine model is proposed. The actuator faults in the pitch subsystems of the wind turbine are regarded as sensor faults. Proposing a bank of SMOs, the output signal is estimated, and the simulated faults are detected and isolated properly.

Several simulation models have been developed for wind turbines by various laboratories around the world. The first verified & validated benchmark model for FDI and FTC purposes was developed by KK-electronic a/c and Aalborg University; it was introduced by Odgaard et al. [3], [8]. Wind turbines are complicated nonlinear systems, and it is very challenging to develop highly accurate models for their subsystems so as to make the FDI process very sophisticated. This benchmark model deals with the wind turbine at a system level and provides the models with enough accuracy for different subsystems of the wind turbine.

Most of the papers concentrating on the FDI of this benchmark model only detect and isolate the faults and scarcely give any information about the fault magnitude. FTC schemes, in particular, require the fault magnitude. The fault diagnosis scheme proposed in this paper can faithfully reconstruct the faults and provide the faults magnitude along with the fault detection and isolation process. In other words, the novelty of this work is the reconstruction of the fault signals and giving information about the fault magnitude. So, the proposed FDD scheme can be used for FTC purposes.

Particularly in this paper, a modified SMO-based fault estimation scheme is presented to detect, isolate, and estimate sensor and actuator faults in the benchmark model subsystems. Some modifications to the discontinuous switching term of the observer are suggested in this paper; they allow the accurate reconstruction of multiple sensors or actuator faults occurring simultaneously. Five fault scenarios are considered in the generator and drive train subsystems, occurring at the rotor speed, generator speed, and generator torque sensors. One of these scenarios simulates the simultaneous fault occurrence. Four fault scenarios are also considered in the pitch and blade subsystems, occurring at pitch hydraulic actuators and pitch angle measurement sensors. The simulations are implemented in the MATLAB Simulink environment by considering sensor faults, actuator faults, and measurement noise. The fault signals are well detected, isolated, and reconstructed by the proposed SMO.

The second validated and verified benchmark model for FDI and FTC purposes was developed by the U.S. National Renewable Energy Laboratory (NREL) [26]. This benchmark incorporates the FAST aero elastic simulator code (fatigue, aerodynamics, structures, and turbulence), which models the WT with 24 degrees of freedom [27]. Since this benchmark is a higher-fidelity and more realistic wind turbine model with some uncertainty sources, it requires more sophisticated and robust FDD schemes. Investigation of robust SMO-based FDD schemes to handle the faults in this benchmark model is regarded as the future work of the authors.

The paper is organized as the following: Section 2 describes the wind turbine benchmark model in brief. The SMO structure is presented in Section 3. The observer design procedure, fault scenarios, and numerical simulation results for the drive train and generator subsystems are described in

Section 4. Section 5 aims at the sensor and actuator fault diagnosis of the pitch subsystem. Finally, Section 6 concludes the paper.

2.Wind turbine benchmark model

The FDI scheme proposed in this paper and the fault scenarios are simulated in a well-known wind turbine benchmark model presented by Odgaard et al. [3], [8]. This is the first validated and verified test benchmark model developed by KK-electronic a/c and Aalborg University to evaluate the fault detection and accommodation schemes. This benchmark model deals with the wind turbine at a system level and provides the models with enough accuracy for different subsystems of the wind turbine.

The system overview of this generic 4.8 MW wind turbine benchmark model is shown in Fig.1, where v_w is the real wind speed, $v_{w,m}$ is the measured wind speed, τ_r is the rotor torque, τ_g is the generator torque, $\tau_{g,m}$ is the measured generator torque, ω_r is the rotor rotational speed, $\omega_{r,m}$ is the measured rotor speed, ω_g is the generator rotational speed, $\omega_{g,m}$ is the measured generator speed, β_r is the blade reference pitch angle, β_m is the measured pitch angle, P_r is the wind turbine nominal power, and P_g is the wind turbine generated power.

Blade & pitch, drive train, generator & converter, and controller are the main subsystems of this three-blade horizontal-axis wind turbine. The wind speed profile has a stochastic manner and is taken from the real measured wind data from a wind park.

2.1.Wind model

In this benchmark model, the wind profile associated with each blade has a stochastic manner and is a bit different from another blade. These stochastic profiles are generated using a wind model that describes the stochastic wind behaviour as well as wind shear effects and tower shadow effects. The input of the wind model is a sequence of real wind speed measurements from a wind park. See [8] for more details.

2.2.Pitch & Blade system

This subsystem includes the aerodynamic model, the wind model, and the pitch model. The aerodynamic torque (τ_r), is calculated using the aerodynamic model by the following expression:

$$\tau_r = \frac{\rho \pi R^3 C_q(\lambda, \beta) v_w^2}{2} \qquad (1)$$

in which R is the radius of the blades, v_w is the wind speed, and $C_q(\lambda, \beta)$ is a mapping of the torque coefficients depending on the tip speed ratio ($\lambda = \frac{R.\omega_r}{v_w}$) and the pitch angle ($\beta$). This mapping is given as a lookup table in the benchmark and is shown in Fig.2.

The hydraulic pitch actuator for each pitch subsystem is modelled by acceptable accuracy using a second-order closed-loop transfer function between the measured pitch angle β and its reference β_r as [8]:

$$\frac{\beta(s)}{\beta_r(s)} = \frac{\omega_n^2}{s^2 + 2.\xi \omega_n.s + \omega_n^2} \qquad (2)$$

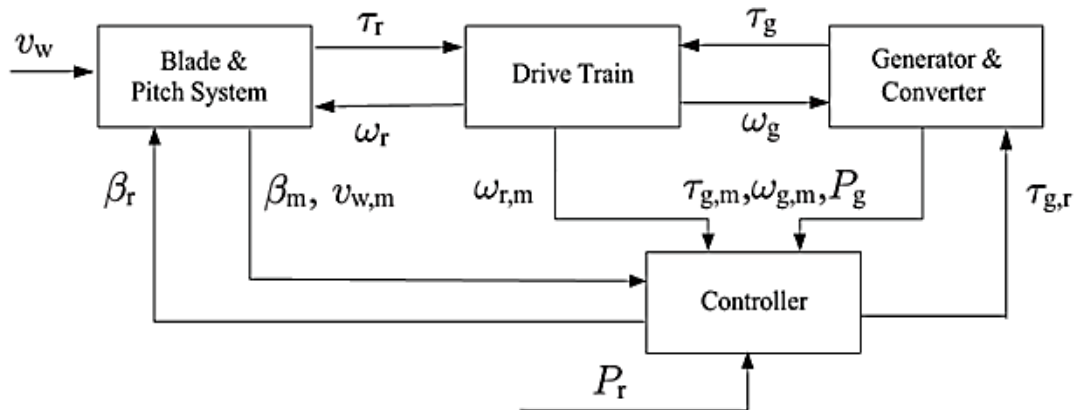β_r is provided by the wind turbine controller.

Fig.1. Overview of the benchmark model [3]

A transfer function is attached to all the three pitch systems. ξ, ω_n are the damping factor and the natural frequency, respectively. In case of no fault, the damping factors are equal for the three pitch systems. In case of fault occurring in a pitch system, the parameters of the faulty system might be different from the others.

2.3.Drive train model

The drive train subsystem aims to transfer the aerodynamic torque from the rotor side to the generator side. The rotational speed from the rotor side to the generator side is increased via a gearbox. The drive train system is modelled by a two-mass spring damper model as the following:

$$J_r \dot{\omega}_r(t) = \tau_{aero}(t) - K_{dt}\theta(t) \tag{3}$$

$$-(B_{dt} + B_r)\omega_r(t) + \frac{B_{dt}}{N_g}\omega_g(t)$$

$$J_g \dot{\omega}_g(t) = \frac{\eta_{dt} K_{dt}}{N_g}\theta(t) \tag{4}$$

$$+\frac{\eta_{dt} B_{dt}}{N_g}\omega_r(t) - \left(\frac{\eta_{dt} B_{dt}}{N_g^2} + B_g\right)\omega_g(t)$$

$$-\tau_{gen}(t)$$

$$\dot{\theta}(t) = \omega_r(t) - \frac{1}{N_g}\omega_g(t) \tag{5}$$

The model parameter definitions are described in Table 1.

2.4.Generator & converter model

At a system level of wind turbine, the generator and converter subsystem can be modelled by a first-order transfer function:

$$\frac{\tau_{gen}(s)}{\tau_{ref}(s)} = \frac{1}{1/\alpha_{gc}s + 1} \tag{6}$$

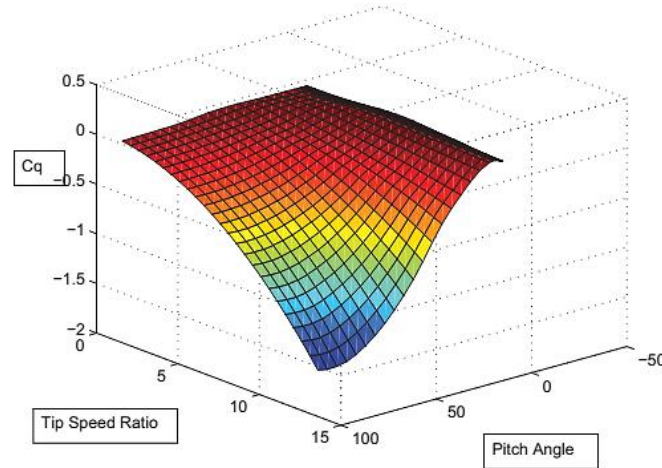in which α_{gc} is the generator and converter model parameter.

Fig.2. Torque coefficient Cq as a function of the tip speed ratio and the pitch angle [8]

Table 1. Parameter description of the drive train [8]

$\omega_r(t)$	$\omega_g(t)$	$\theta(t)$
Rotor speed	Generator speed	Torsion angle of the drive train
$\tau_{aero}(t)$	$\tau_{gen}(t)$	J_r
Rotor torque	Generator torque	Rotor moment of inertia
N_g	η_{dt}	J_g
Gear ratio	Efficiency of the drive train	Generator moment of inertia
B_r	B_g	K_{dt}
Rotor viscous friction	Generator viscous friction	Torsion stiffness of the drive train
B_{dt}		
Torsion damping of the drive train		

3.Sliding mode Observer design

The fault estimation scheme employed in this paper relies on the SMO structure proposed by Edwards et al. [21], [28, ch. 4], which provides real-time estimation of sensor and actuator faults. It is briefly described in the following:

Consider the linear system subject to actuator and sensor faults described by

$$\dot{z}(t) = Az(t) + Bu(t) + Df_{act}(t) \qquad (7)$$

$$y(t) = Cz(t) + f_{sen}(t) \qquad (8)$$

It is argued in [21] that there is a linear change of coordinates $z \to T_z z$ in such a way that in the new coordinate system

$$\dot{z}_1(t) = \mathbb{A}_{11}z_1(t) + \mathbb{A}_{12}z_2(t) \\ + B_1 u(t) \qquad (9)$$

$$\dot{z}_2(t) = \mathbb{A}_{21}z_1(t) + \mathbb{A}_{22}z_2(t) \\ + B_2 u(t) + D_2 f_{act}(t) \qquad (10)$$

$$y(t) = z_2(t) \qquad (11)$$

Referring to [20, Section 4.3], $T_z = T_* T$. The system of (7) and (8) are first transformed by the matrix T and then the second transformation is done by T_*. T and T_* are computed from (12) and (13). T_0 is a p*p orthogonal matrix as (14), where $B_m \in \mathbb{R}^{m*m}$. $T_{12} \in \mathbb{R}^{n-p*p}$ is determined by solving the matrix equation $D_1 + T_{12}D_2 = 0$ and $L_* = [L \ 0]$. More details can be found in [20, 21]

$$T = \begin{bmatrix} I_{n-p} & T_{12} \\ 0 & T_0 \end{bmatrix} \qquad (12)$$

$$T_* = \begin{bmatrix} I_{n-p} & L_* \\ 0 & T_0^T \end{bmatrix} \qquad (13)$$

$$T_0 D_2 = \begin{bmatrix} 0 \\ B_m \end{bmatrix} \qquad (14)$$

After applying the change of coordinate (T_z) and rewriting the system of Eqs. (7), (8) in the canonical form of (9)–(11), the observer finally has the structure of Eq. (15), where e_y is the output estimation error, v is the sliding term (as Eq.(16)), and G_e, G_v are the design matrices (as Eq.(17)).

$$\dot{\hat{z}}(t) = A\hat{z}(t) + Bu(t) - G_e e_y(t) \\ - G_v v \qquad (15)$$

$$v = \begin{cases} \gamma \parallel D_2 \parallel \dfrac{Pe_y}{\parallel Pe_y \parallel} & if \ e_y \neq 0 \\ 0 & otherwise \end{cases} \qquad (16)$$

$$G_e = T_z{}^{-1} \begin{bmatrix} \mathbb{A}_{12} \\ \mathbb{A}_{22} - \mathbb{A}^S{}_{22} \end{bmatrix}$$

$$\text{and} \ \ G_v = T_z{}^{-1} \begin{bmatrix} 0 \\ I_p \end{bmatrix} \qquad (17)$$

$$\hat{f}_{act}(t) \approx -\gamma \parallel D_2 \\ \parallel (D_2^T D_2)^{-1} D_2^T \dfrac{Pe_y}{\parallel Pe_y \parallel + \delta} \qquad (18)$$

$$\hat{f}_{sen}(t) \approx (\mathbb{A}_{22} - \mathbb{A}_{21}\mathbb{A}_{11}^{-1}\mathbb{A}_{12})^{-1}\gamma \\ \parallel D_2 \parallel \dfrac{Pe_y}{\parallel Pe_y \parallel + \delta} \qquad (19)$$

$\mathbb{A}^S{}_{22}$ is a stable design matrix; P is a Lyapunov matrix for $\mathbb{A}^S{}_{22}$; and the scalar γ is the upper bound of the fault. Finally, the actuator and sensor faults are reconstructed using the so-called 'equivalent output error injection' as Eqs. (18),(19). For more details,

3.1.Modifications to the switching term

Some modifications to the switching term (16) are suggested in this paper to enhance the accuracy of the fault reconstruction. The rotor speed, the generator speed, and the generator torque are measured with the appropriate sensors, and they are considered as the system outputs. These sensor outputs are of the order of the magnitude of 1, 1e2, and 1e4, respectively. Consequently, the faults occurring in these sensors differ in magnitude. Also, the elements of the output estimation error vector (e_y) have different magnitudes. For the occurrence of the sliding motion, the proper choice of γ is crucial and the accuracy of the fault reconstruction is highly dependent on the proper selection of the scalar γ. In case multiple sensor faults occur in the system, the discontinuous switching term with the structure of (16) imposes a limitation on the fault reconstruction and all the faults are not estimated correctly with this structure. To address this problem, two modifications are suggested in this paper.

1- The output estimation error e_y is replaced with a weighted one: $W_e e_y$, where the weighting matrix W is a diagonal matrix with a reciprocal of the average values of the output components as $W_e = \text{diag}(W_{e1}, \dots, W_{ep}) = \text{diag}(1/y_{1,ave}, \dots, 1/y_{p,ave})$. With this modification, the components of the modified output estimation error $W_e e_y$ become the comparable order of magnitude.

The term W_e aims at scaling the output estimation error. Since the stochastic wind speed considered in this paper is the full load speed, $y_{I,average}$ is considered as equal to the nominal value of the i-th output in the full load region., i.e

$y_{1,average} = 1.7 \frac{rad}{sec}$,

$y_{2,average} = 160 \frac{rad}{sec}$,

$y_{3,average} = 3.4e^4 \, N.m.$

2- The scalar gain γ is replaced by a positive definite diagonal matrix: $\Upsilon = \text{diag}(\gamma_1, \dots, \gamma_p)$. This modification suggests the individual gains for faults with a different order of magnitude.

These modifications scale the output estimation error and set a private gain for each fault. This leads to the accurate reconstruction of all faults when multiple sensors with different orders of measurements are faulty. By applying these modifications, the switching term υ is revised as:

$$\upsilon = \begin{cases} \Upsilon \parallel D_2 \parallel \dfrac{PW_e e_y}{\parallel PW_e e_y \parallel} & if \ e_y \neq 0 \\ 0 & otherwise \end{cases} \quad (20)$$

For simulation, a continuous form of υ is utilized. The reconstruction of the actuator and sensor faults are modified as:

$$\hat{f}_{act}(t) \approx -\Upsilon \parallel D_2 \quad (21)$$
$$\parallel (D_2^T D_2)^{-1} D_2^T \frac{PW_e e_y}{\parallel PW_e e_y \parallel + \delta}$$

$$\hat{f}_{sen}(t) \approx (\mathbb{A}_{22} - \mathbb{A}_{21}\mathbb{A}_{11}^{-1}\mathbb{A}_{12})^{-1}\Upsilon$$
$$\parallel D_2$$
$$\parallel \frac{PW_e e_y}{\parallel PW_e e_y \parallel + \delta} \quad (22)$$

4. Drive train and generator sensor fault reconstruction

Considering the benchmark drive train and generator models, the state space of the system, including the sensor faults, can be written as:

$$\begin{Bmatrix} \omega_{g_m} \\ \omega_{r_m} \\ \tau_{g_m} \end{Bmatrix} = \begin{bmatrix} 1 & 0 & 0 & 0 \\ 0 & 1 & 0 & 0 \\ 0 & 0 & 0 & 1 \end{bmatrix} \begin{Bmatrix} \omega_g \\ \omega_r \\ \theta \\ \tau_{gen} \end{Bmatrix} + \begin{Bmatrix} f_{\omega_g} \\ f_{\omega_r} \\ f_{\tau_{gen}} \end{Bmatrix} \quad (24)$$

where ω_{g_m} is the measurement of the generator speed, f_{ω_g} is the generator speed sensor fault, ω_{r_m} is the measurement of the rotor speed, f_{ω_r} is the rotor speed sensor fault, τ_{g_m} is the measurement of the generator torque, and $f_{\tau_{gen}}$ is the generator torque sensor fault.

4.1 Observer design

Regarding the system representation of Eqs. (23) and (24), as compared with Eqs. (7) and (8), there were attempts to design an SMO to estimate the sensor faults ($f_{sen}(t)$), i.e., f_{ω_g}, f_{ω_r}, $f_{\tau_{gen}}$. In this section, $f_{act}(t)$ is equal to zero. It should be noted that τ_{ref} (the second input in [23]) is provided by the wind turbine controller. The aerodynamic torque, τ_{aero}, is the main source of excitation of the system, which causes the WT to rotate. This torque is determined from Eq.(1) as the observer first input.

The proposed SMO observer has the structure of (15) with the modified weighted switching term as (20) and the sensor fault reconstruction vector as (19) Using an algorithm similar to the one proposed in [20], it can finally be shown that the system described in Eqs. (23) and (24) is transformed into a canonical form with the state space matrices:

$$\mathbb{A} = \begin{bmatrix} -6.36e5 & 0.82 & -5.73e6 & 0.023 \\ -49.1 & -1.4e-5 & -441.8 & 0 \\ 7.07e4 & 0.0203 & 6.36e5 & -0.0026 \\ 0 & 0 & 0 & -50 \end{bmatrix}$$

$$\begin{Bmatrix} \dot{\omega}_g \\ \dot{\omega}_r \\ \dot{\theta} \\ \dot{\tau}_{gen} \end{Bmatrix} = \begin{bmatrix} -\dfrac{\left(\frac{\eta_{dt}B_{dt}}{N_g^2} + B_g\right)}{J_g} & \dfrac{\eta_{dt}B_{dt}}{N_g J_g} & \dfrac{\eta_{dt}K_{dt}}{N_g J_g} & -\dfrac{1}{J_g} \\ \dfrac{B_{dt}}{N_g J_r} & -\dfrac{(B_{dt} + B_r)}{J_r} & -\dfrac{K_{dt}}{J_r} & 0 \\ -\dfrac{1}{N_g} & 1 & 0 & 0 \\ 0 & 0 & 0 & -\alpha_{gc} \end{bmatrix} \begin{Bmatrix} \omega_g \\ \omega_r \\ \theta \\ \tau_{gen} \end{Bmatrix} + \begin{bmatrix} 0 & 0 \\ \frac{1}{J_r} & 0 \\ 0 & 0 \\ 0 & \alpha_{gc} \end{bmatrix} \begin{Bmatrix} \tau_{aero} \\ \tau_{ref} \end{Bmatrix} \quad (23)$$

$$\mathbb{B} = \begin{bmatrix} 0 & 0 \\ 1.82e-8 & 0 \\ 0 & 0 \\ 0 & 50 \end{bmatrix},$$

$$\mathbb{C} = \begin{bmatrix} 0 & 1 & 0 & 0 \\ 0 & 0 & 1 & 0 \\ 0 & 0 & 0 & 1 \end{bmatrix},$$

$$\mathbb{D} = \begin{bmatrix} 0 \\ 1.82e-8 \\ 0 \\ 0 \end{bmatrix} \qquad (25)$$

The observer design parameters are considered as:

$$\mathbb{A}^s{}_{22} = diag\{-4e2; -5e2; -6e2\},$$
$$\Upsilon = diag\,(2e2, 3e4, 5e6\,),$$
$$W_e = diag\left(\frac{1}{1.7}, \frac{1}{160}, \frac{1}{3.4e^4}\right), \text{ and } \delta = 1e^{-3}.$$

The proposed observer is used to reconstruct the sensor faults in various scenarios. Assuring that the sliding motion has occurred, the sensor faults are reconstructed using the '*equivalent output error injection signal*' from (19). The sensor fault scenarios are described in the following section.

4.2 Fault scenarios and wind input

The drive train and generator model parameters are like the benchmark ones and are listed in Table 2. A stochastic wind input profile, taken from the real wind speed measurement of a wind park [8], is used in the simulation and illustrated in Fig.3. All five representative sensor fault cases, as Table 3, are simulated in the benchmark model.

Simulations for the fault cases 1–1 to 1–4 are in the absence of measurement noise, while in the fault case 1–5 measurement noise is present.

4.3 Simulation results

Fault case 1–1
Figure 4 shows the actual and estimated fault values in an intermittent fault scenario starting from 2s and ending at 5s. This fault case realizes the variable amplitude constant bias in the generator torque sensor. Estimation overshoots or undershoots at the time of changing the fault magnitude, but the estimation immediately reaches the actual value as the dynamics of the observer is very fast. It is seen that the accurate reconstruction of the fault signal is provided by the proposed observer.

Fault case 1–2
The generator speed sensor fault is simulated to start from 17s and end at 25s as Fig.5 (fault case 1–2). The reconstructed fault by SMO chatters a little around the actual fault, but provides a relatively accurate estimation.

Fault case 1–3
The rotor speed sensor experiences an intermittent bias fault starting from 27s and ending at 30s. Figure 6 shows the simulated fault compared to the estimated one in which sufficiently good estimation is observed.

Fault case 1–4
To prove the effectiveness of modifying the

Table 2. Drive train and generator model parameters [8]

$B_{dt}\left(\dfrac{Nms}{rad}\right)$	$B_r\left(\dfrac{Nms}{rad}\right)$	$B_g\left(\dfrac{Nms}{rad}\right)$	N_g	$K_{dt}\left(\dfrac{Nm}{rad}\right)$
775.49	7.11	45.6	95	$2.7\,.\,10^9$
η_{dt}	$J_r(\text{kg.}\,\text{m}^2)$	$J_g(\text{kg.}\,\text{m}^2)$	$\alpha_{gc}\left(\dfrac{rad}{sec}\right)$	
0.97	$55\,.\,10^6$	390	50	

Table 3. List of the simulated faults in the drive train and generator subsystems

Fault case	Description
Fault case 1–1	Rectangular intermittent fault in the generator torque sensor
Fault case 1–2	Saw tooth fault in the generator speed sensor
Fault case 1–3	Rectangular intermittent fault in the rotor speed sensor
Fault case 1–4	Simultaneous biases in all sensors
Fault case 1–5	Generator speed sensor fault in the presence of measurement noise

switching term, a simultaneous scenario is considered. The fault case 1–4 suggests a scenario in which the sensor faults occur simultaneously. A bias of 1000 N.m in the generator torque sensor within 32s–38s, a bias of 20 rad/sec in the generator speed sensor within 34s–38s, and a bias of -0.2 rad/sec in the rotor speed sensor within 36s–38s are simulated in the benchmark model. For all sensors, the estimated faults reveal a high agreement with the actual ones, although a little variation exists at 32s, 34s, and 36s (starting a new fault). An SMO with an unmodified switching term such as (16) can never faithfully estimate all the simulated simultaneous faults. The simulated and estimated faults for the generator torque sensor are shown in Fig.7.

All the already simulated faults are in the absence of measurement noise. Considering the benchmark generator speed sensor noise with a standard deviation of 0.05 rad/sec, an intermittent simulated fault, compared to the estimated one, is reported as Fig.8. The fault signal is well reconstructed even at the presence of measurement noise. Since the designed observer does not decouple the sensor fault from sensor noise, the measurement noise is reflected in the reconstructed fault. So, the estimated fault is passed through an appropriate low-pass filter to reduce the noise effect. Although the low-pass filter implies a little delay on the estimation, it considerably reduces the noise effect. Similarly, sufficiently good reconstruction of fault signals is achieved for rotor speed and generator torque sensors in the presence of measurement noise.
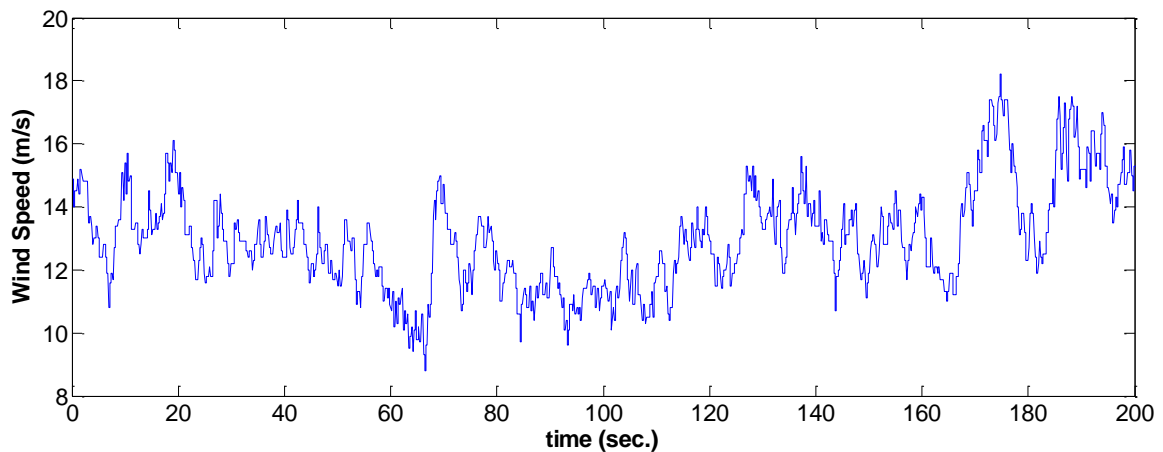

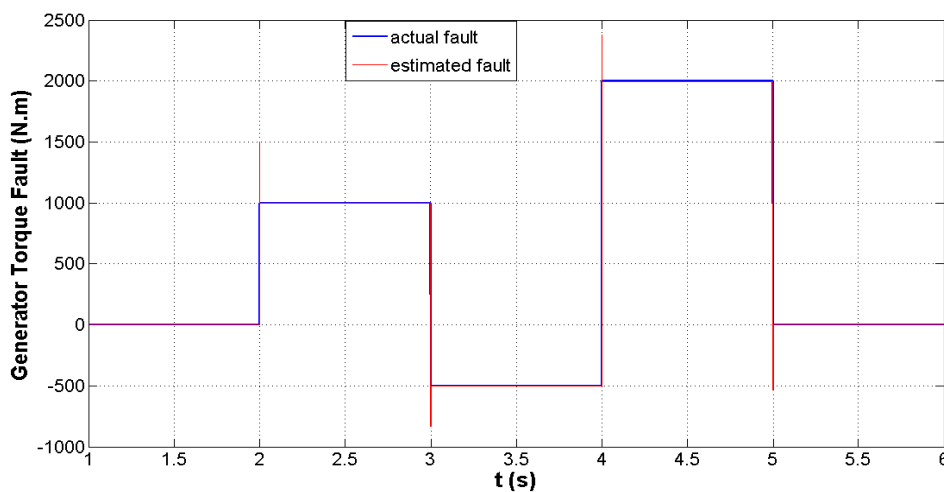**Fig.3.** Stochastic wind speed profile used in the simulations

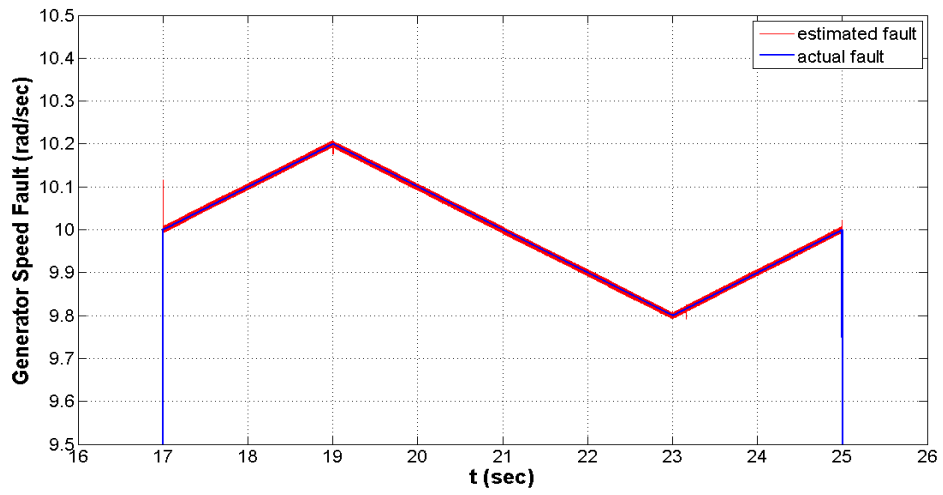**Fig.4.** Generator torque sensor simulated and real-time estimated faults (fault case 1−1)

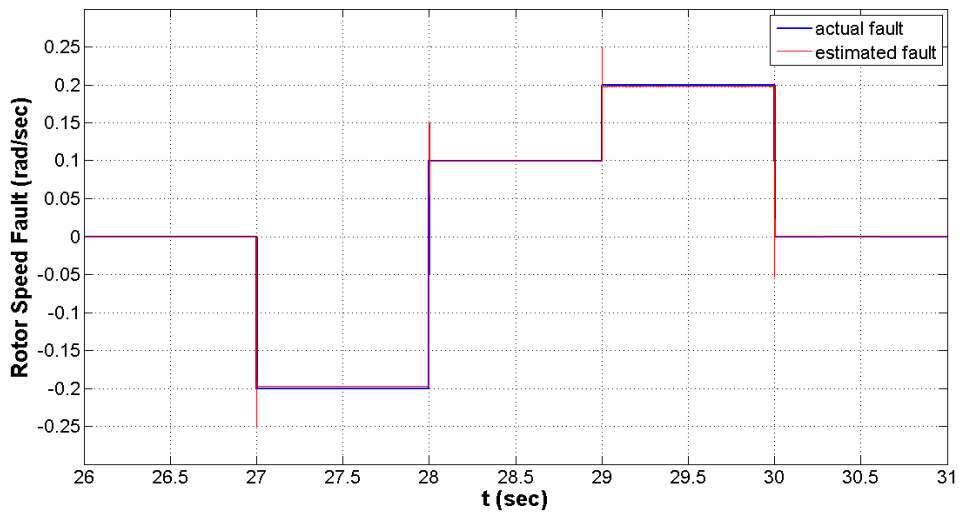**Fig.5.** Generator speed sensor simulated and real-time estimated faults (fault case 1–2)

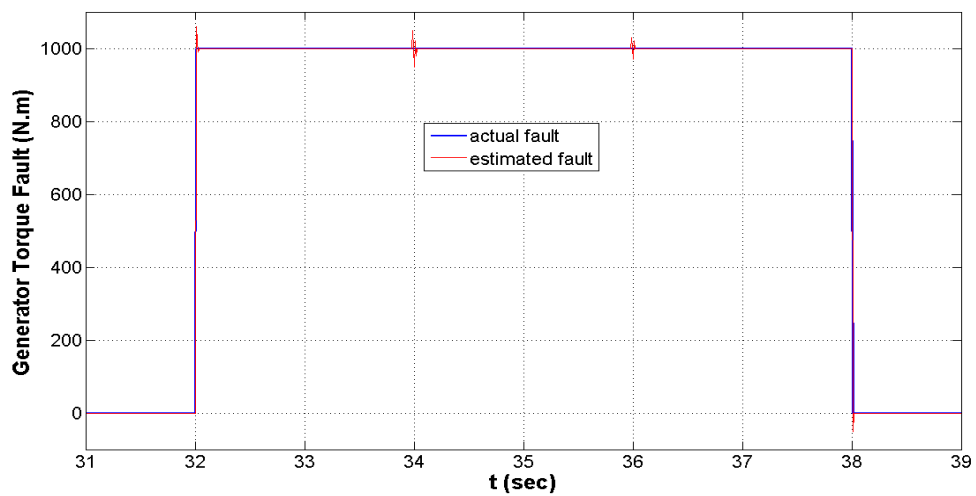**Fig. 6.** Rotor speed sensor simulated and real-time estimated faults (fault case 1–3)

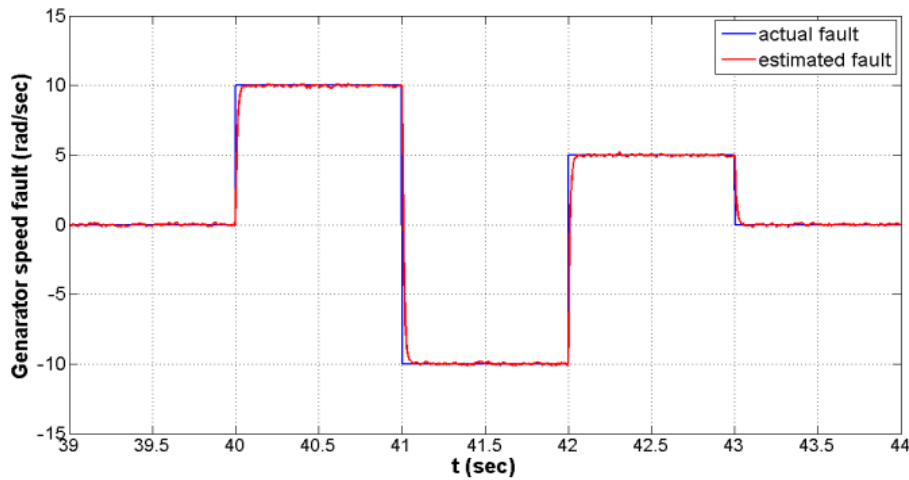**Fig.7.** Generator torque sensor simulated and real-time estimated faults (fault case 1–4)

Fig.8. Generator speed sensor actual and estimated faults in the presence of measurement noise (fault case 1–5)

5.Pitch subsystem fault diagnosis

In this section, fault diagnosis of pitch actuators and sensors is investigated. In fault-free conditions, ξ and ω_n are assumed to be the same for three pitch actuators. However, in case of a fault in a pitch actuator, these parameters are different from one pitch actuator to another. In order to model the hydraulic power abrupt drop in a pitch actuator, these parameters in the transfer function are changed to ω_{n2} and ξ_2. In this paper, these parameters are considered as: $\xi = 0.6$, $\omega_n = 11.11\ rad/sec$, $\xi_2 = 0.45$, and $\omega_{n2} = 5.73\ rad/sec$ [8].

5.1 Fault detection and isolation scheme

First, some sensor residual signals are defined as:

$$r_{ij}(t) = \beta_{im}(t) - \beta_{jm}(t)\ ,i \neq j \qquad (26)$$

where β_{im} is the i-th pitch subsystem position measurement. To minimize the effect of measurement noise, the residuals are passed through appropriate low-pass filters. The

the actuator fault eventually affects the measurement of the pitch angle, some of residuals deviate significantly from zero. For instance, the occurrence of faults in pitch actuator 1 results in r_{12}, r_{13}, r_{21} and r_{31} deviating significantly from zero. So, when the residuals deviate significantly from zero, it means that a certain fault has occurred in the system.

Recalling from the Eq.(1), the aerodynamic torque is a function of the pitch angle. Consider the between these situation when a fault occurs in one of the pitch actuators, the produced aerodynamic torque (so-called $\tau_{aero-faulty}$) would be different from the aerodynamic torque in the fault-free condition (so-called $\tau_{aero-healthy}$). The difference between these torques constitutes the aerodynamic torque fault ($\tau_{aero-faulty} = \tau_{aero-healthy} + f_{\tau_{aero}}$), which is caused by a fault in the pitch actuator. In faulty conditions, the aerodynamic torque entering the state space is a faulty torque and hence the state space Eq. (23) can be rewritten as:

$$\begin{Bmatrix} \dot{\omega}_g \\ \dot{\omega}_r \\ \dot{\theta} \\ \dot{\tau}_{gen} \end{Bmatrix} = \begin{bmatrix} -\dfrac{\left(\dfrac{\eta_{dt}B_{dt}}{N_g^2} + B_g\right)}{J_g} & \dfrac{\eta_{dt}B_{dt}}{N_gJ_g} & \dfrac{\eta_{dt}K_{dt}}{N_gJ_g} & -\dfrac{1}{J_g} \\ \dfrac{B_{dt}}{N_gJ_r} & -\dfrac{(B_{dt}+B_r)}{J_r} & -\dfrac{K_{dt}}{J_r} & 0 \\ -\dfrac{1}{N_g} & 1 & 0 & 0 \\ 0 & 0 & 0 & -\alpha_{gc} \end{bmatrix} \begin{Bmatrix} \omega_g \\ \omega_r \\ \theta \\ \tau_{gen} \end{Bmatrix} + \begin{bmatrix} 0 & 0 \\ \dfrac{1}{J_r} & 0 \\ 0 & 0 \\ 0 & \alpha_{gc} \end{bmatrix} \begin{Bmatrix} \tau_{aero-helathy} \\ \tau_{ref} \end{Bmatrix} + \begin{bmatrix} 0 \\ \dfrac{1}{J_r} \\ 0 \\ 0 \end{bmatrix} f_{\tau_{aero}} \qquad (27)$$

reference pitch angle is the same for all pitch subsystems and hence r_{ij} tends to zero in fault-free conditions. Since the occurrence of

Comparing Eq. (27) with Eq. (7), $f_{\tau_{aero}}$ is regarded as the actuator fault and the proposed SMO can estimate it in faulty

conditions. The method of computing $\tau_{aero-helathy}$ as the observer input is relatively simple. Passing the pitch reference angle through the pitch actuator transfer function of (2), the pitch angle in healthy conditions is obtained. Considering the pitch angle, wind speed, and rotor speed, the healthy torque can be determined from the aerodynamic model of (1).

To establish a criterion in order to detect the fault occurrence, some fault indicators are defined as:

$$R_{ij}(t) = \int_{t-\Delta t}^{t} |r_{ij}(\delta)|d\delta , F_{\tau_{aero}}(t)$$
$$= \int_{t-\Delta t}^{t} |\hat{f}_{\tau_{aero}}(\delta)|d\delta \qquad (28)$$

where |.| stands the absolute value. Δt is selected to be 0.5s and a threshold value of 0.03 is considered. In fault-free conditions, the fault indicators never exceed the appropriately considered threshold. Whenever the threshold is exceeded by at least one of the fault indicators, the FDI module gives an alarm and the fault is detected. By investigating the values of fault indicators in fault-free conditions and extensive fault scenarios (including the faults shown in Table 4), it was found that the value of 0.03 is appropriate and leads to correct and fast fault

detection. A threshold less than 0.03 may lead to false alarm and more than 0.03 deteriorates the fast fault detection and the fault is detected with more delay than now.

The isolation strategy is based on the use of the aerodynamic torque fault estimated by the SMO. In detail, when a fault occurs in one of the pitch actuators, the aerodynamic torque fault, $f_{\tau_{aero}}$ in Eq.(27), deviates significantly from zero. Then, the following fault isolation strategy is established:

- If $F_{\tau_{aero}}$ does not exceed the threshold and R_{ij} exceeds the threshold while R_{jk} does not exceed, then the i-th sensor is faulty.
- If $F_{\tau_{aero}}$ exceeds the threshold and R_{ij} exceeds the threshold while R_{jk} does not exceed, then the i-th actuator is faulty.

where $i, j, k \in \{1,2,3\}, i \neq j \neq k$. Following the isolation strategy, the fault is properly isolated and r_{ij} approximately represents the sensor/actuator fault magnitude. The fault diagnosis scheme implemented in this paper is illustrated in Fig.9.

5.2 Fault scenarios and simulation results

In order to evaluate the FDI module, four representative fault cases are considered in the pitch subsystems in Table 4. The results are presented in the following.
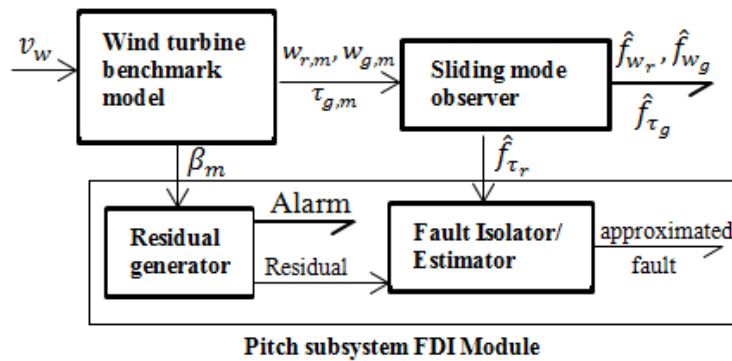

Fig. 9. The fault diagnosis scheme

Table 4. List of the considered faults in the pitch subsystem

Fault case	Description
Fault case 2–1	Dynamics change (abrupt pressure drop) of pitch actuator 3 –from 10th to 20th sec.
Fault case 2–2	Intermittent rectangular faults on pitch actuator 1–from 25th to 40th sec.
Fault case 2–3	Gain factor on pitch sensor 1, equal to 1.2–from 45th to 50th sec.
Fault case 2–4	Intermittent bias on pitch sensor 2–from 52th to 63th sec

Fault case 2–1 considers a fast change in the dynamics of actuator 3 implemented within 10th–20th seconds. This change makes the pitch angle differ from its true value and causes a fault on the pitch angle. During this fault, some of fault indicators exceed the threshold. The fault indicators R_{31}, R_{12}, and $F_{\tau_{aero}}$ are illustrated in Fig.10. The fault is immediately detected at the 10th second, since $F_{\tau_{aero}}$ exceeds the threshold. Following the isolation strategy, R_{31} and $F_{\tau_{aero}}$ exceed the threshold, while R_{12} does not; hence, there is a fault in pitch actuator 3.

Fault case 2–2 realizes an intermittent rectangular fault in pitch actuator 1 within the 25th–40th seconds. The fault indicators R_{12}, R_{23}, and $F_{\tau_{aero}}$ are illustrated in Fig.11. The fault is immediately detected at 25th sec as $F_{\tau_{aero}}$ exceeds the threshold. R_{12} and $F_{\tau_{aero}}$ exceed the threshold, while R_{23} does not do so, and, hence, it is clear that a fault has occurred in pitch actuator 1. The reconstructed fault, reflected in r_{12}, is very close to the simulated one, and both are shown in Fig.12.

In fault case 2–3, a gain factor of 1.2 is applied to the pitch sensor 1 measurements within the 45th–50th seconds. Exceeding the

In fault case 2–3, again factor of 1.2 is

applied to the pitch sensor 1 measurements within the 45th–50th seconds. Exceeding the threshold by R_{12} at 45.22 second, the fault is detected. Exceeding the threshold only by R_{12} means the pitch sensor 1 experiences a fault (see Fig.13).

An intermittent bias fault is simulated in the pitch sensor 2 measurements as fault case 2–4 within the 52th-63th seconds. The fault is detected at 52.03 second. The simulated and estimated faults are depicted in Fig.14 also.

In all simulated scenarios, the proposed fault diagnosis scheme immediately detects and isolates the faults, and then, provides sufficiently good reconstruction of fault signals.

6.Conclusion

This paper describes the development of a fault diagnosis scheme that exploits a sliding mode observer with a modified switching term and residual generation method in order to estimate some sensor and actuator faults in a well-known wind turbine benchmark model. Five fault scenarios are considered in the rotor speed, generator speed, and generator torque sensors, and four fault scenarios are simulated in the pitch subsystems sensors, and actuators. The simulation results show that the proposed diagnosis scheme provides an accurate
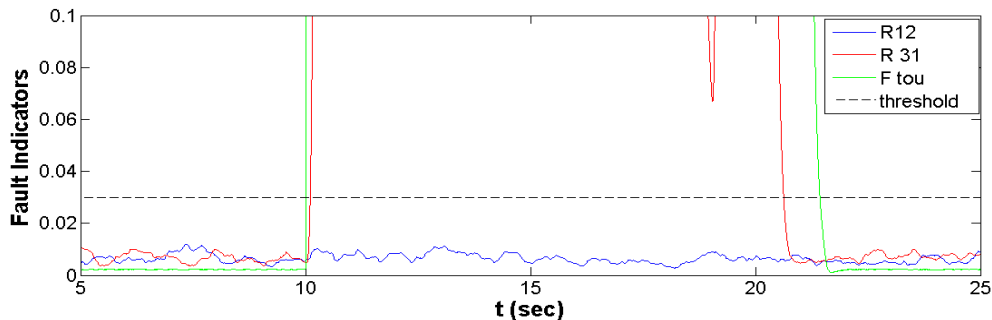

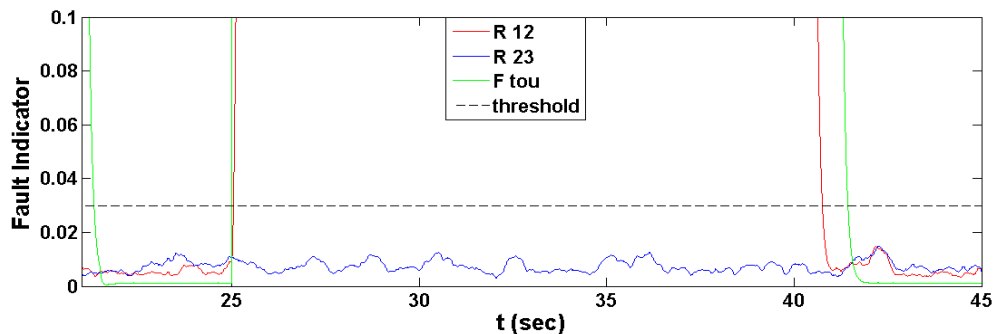**Fig.10.** Fault indicators during the occurrence of fault case 2–1

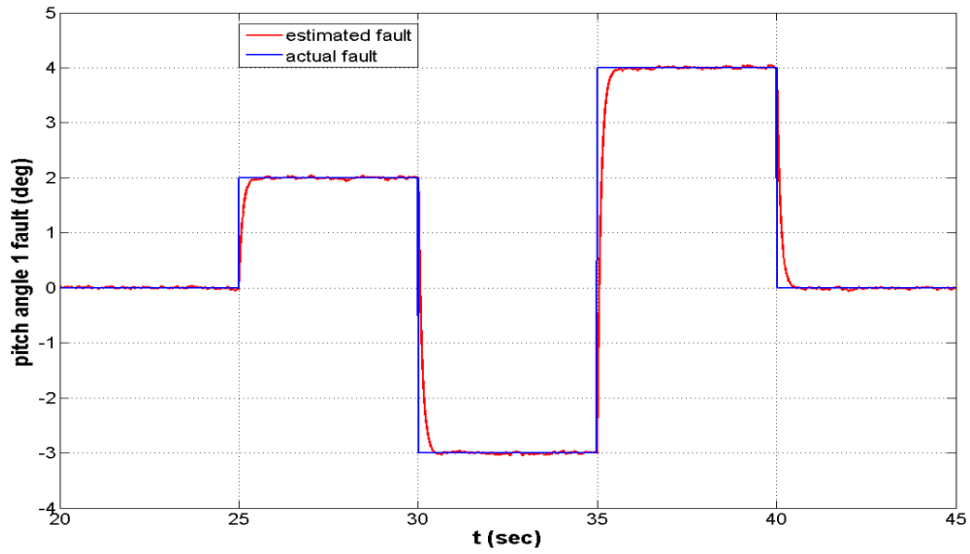**Fig.11.** Fault indicators during the occurrence of fault case 2–2

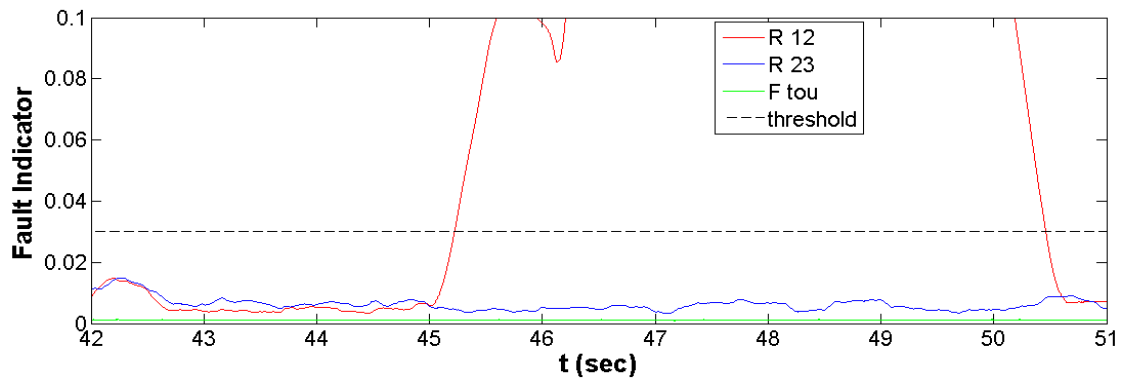**Fig.12.** Simulated and estimated faults on the pitch actuator 1

Fig.13. Fault indicators during the occurrence of fault case 2–3
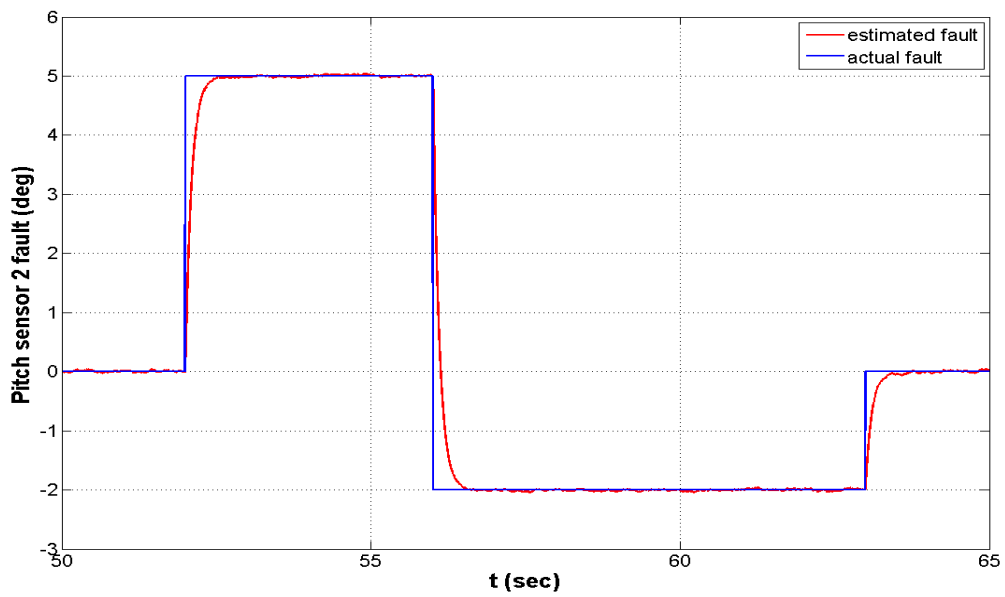

Fig.14. Intermittent rectangular faults in the pitch sensor 2

detection, isolation, and reconstruction of fault signals in the presence of measurement noise. Investigation of the robust SMO-based FDD schemes to handle the faults in a more realistic benchmark model incorporated with FAST is suggested as a good direction for further research, and it is intended in the author's future work.

References

[1] World Wind Energy Report (2016).

[2] Wu B., Lang Y., Zargari N., Kouro S., Power Conversion and Control of Wind Energy Systems. Wiley-IEEE Press (2011).

[3] Odgaard P. F., Stoustrup J., Kinnaert M., Fault Tolerant Control of Wind Turbines –A Benchmark Model, In 7th IFAC Symposium on Fault Detection, Supervision and Safety of Technical Processes (2009) 155–160.

[4] Esbensen T., Sloth C., Fault Diagnosisand Fault-Tolerant Control of Wind Turbines, Aalborg University, Aalborg, Denmark (2009).

[5] Badihi H., Zhang Y., Hong H., A Review on Application of Monitoring, Diagnosis and Fault- Tolerant Control to Wind Turbines, In 2013 Conference on Control and Fault-Tolerant Systems (2013) 365–370.

[6] Hameed Z., Hong Y. S., Cho Y. M., Ahn S. H., Song C. K., Condition Monitoring and Fault Detection of Wind Turbines and Related Algorithms, A Review, Renewable and Sustainable Energy Reviews (2009) 13:1–39,.

[7] Lu B., Li Y., Wu X., Yang Z., A Review of Recent Advances in Wind Turbine Condition Monitoring and Fault Diagnosis, In IEEE Conference on Power Electronics and Machines in Wind Applications (2009) 1–7.

[8] Odgaard P. F., Stoustrup J., Kinnaert M., Fault-Tolerant Control of Wind Turbines, A Benchmark Model, IEEE Transactions on Control Systems Technology (2013) 21(4): 1168–1182.

[9] Chen W., Ding S. X., Haghani A., Naik A., Khan A. Q., Yin S., Observer-Based FDI Schemes for Wind Turbine Benchmark, In 18th IFAC World Congress (2011) 7073–7078.

[10] Kiasi F., Prakash J., Shah S. L., Lee J. M., Fault Detection and Isolation of a Benchmark Wind Turbine Using the Likelihood Ratio Test, In 18th IFAC World Congress (2011) 7079–7085.

[11] Laouti N., Othman S., Alamir M., Sheibat-Othman N., Combination of Model-based Observer and Support Vector Machines for Fault Detection of Wind Turbines, International Journal of Automation and Computing (2014) 11(3):274–287.

[12] Pisu P., Ayalew B., Robust Fault Diagnosis for a Horizontal Axis Wind Turbine," in 18th IFAC World Congress, Italy (2011) 2(1): 7055–7060.

[13] Tabatabaeipour S. M., Odgaard P. F., Bak T., J. Stoustrup, Fault Detection of Wind Turbines with Uncertain Parameters, A Set- Membership Approach, Energies (2012) 5: 2424–2448.

[14] Hernández J., Guadayol M., España A. R., Wind Speed Estimation in Wind Turbines Using EKF, Application to Experimental Data, In 2014 UKACC International Conference on Control (2014) 474–479.

[15] Jena D., Rajendran S., A Review of Estimation of Effective Wind Speed Based Control of Wind Turbines, Renewable & Sustainable Energy Reviews (2015) 43: 1046–1062.

[16] Odgaard P. F., Stoustrup J., Nielsen R., Damgaard C., Observer Based Detection of Sensor Faults In Wind Turbines, In Proceedings of European Wind Energy Conference (2009) 1–10.

[17] Odgaard P. F., Stoustrup J., Unknown Input Observer Based Detection of Sensor Faults in a Wind Turbine, In Proceedings of the IEEE Multiconference on Systems and Control (2010) 310–315.

[18] Simani S., Farsoni S., Castaldi P., Robust Actuator Fault Diagnosis of a Wind Turbine Benchmark Model, In 52nd IEEE Conference on Decision and Control, (2013) 4422–4427.

[19] Simani S., Castaldi P., Active Actuator Fault-Tolerant Control of a Wind Turbine Benchmark Model, International Journal ROBUST NONLINEAR Control (2014) 24:1283–1303.

[20] Edwards C., Spurgeon S. K., On the Development of Discontinuous Observers, International Journal of Control (1994) 59(5): 1211–1229.

[21] Edwards C., Spurgeon S. K., Patton R. J., Sliding Mode Observers for Fault Detection and Isolation, Automatica (2000) 36: 541–553.

[22] Tan C. P., Edwards C., Sliding Mode Observers for Detection and Reconstruction of Sensor Faults, Automatica (2002) 38(10): 1815–1821.

[23] Tan C. P., Edwards C., Sliding Mode Observers for Robust Detection and Reconstruction of Actuator and Sensor Faults, International Journal of Robust Nonlinear Control (2003) 13(5): 443–463.

[24]Im J. S., Ozaki F., Yeu T. k., Kawaji S., Model-Based Fault Detection and Isolation in Steer- by- Wire Vehicle Using Sliding Mode Observer, Journal of Mechanical Science and Technology (2009) 23(8):1991–1999.

[25]Zhang J., Bennounat O., Swaint A. K., Nguangt S. K., "Detection and Isolation of Sensor Faults of Wind Turbines using Sliding Mode Observers," in Renewable and Sustainable Energy Conference (IRSEC) (2013)(1).

[26] Odgaard P. F., Johnson K. E., Wind Turbine Fault Detection and Fault Tolerant Control - An Enhanced Benchmark Challenge," in 2013 American Control Conference (2013) 4447–4452.

[27] Jonkman J., Buhl M. L., FAST User ' s Guide, NREL/EL-500-38230, Golden, CO (2005).

[28] Halim A., Edwards C., Tan C. P., Fault Detection and Fault-Tolerant Control Using Sliding Modes, Springer-Verlag London (2011).